



Tropical climate and vegetation changes during Heinrich Event 1: a model-data comparison

D. Handiani^{1,2}, A. Paul^{1,2}, and L. Dupont¹

¹MARUM – Center for Marine Environmental Sciences, University of Bremen, 28359 Bremen, Germany

²Department of Geosciences, University of Bremen, Bremen, Germany

Correspondence to: D. Handiani (dhandiani@marum.de)

Received: 31 May 2011 – Published in Clim. Past Discuss.: 21 June 2011

Revised: 5 November 2011 – Accepted: 8 November 2011 – Published: 4 January 2012

Abstract. Abrupt climate changes from 18 to 15 thousand years before present (kyr BP) associated with Heinrich Event 1 (HE1) had a strong impact on vegetation patterns not only at high latitudes of the Northern Hemisphere, but also in the tropical regions around the Atlantic Ocean. To gain a better understanding of the linkage between high and low latitudes, we used the University of Victoria (UVic) Earth System-Climate Model (ESCM) with dynamical vegetation and land surface components to simulate four scenarios of climate-vegetation interaction: the pre-industrial era, the Last Glacial Maximum (LGM), and a Heinrich-like event with two different climate backgrounds (interglacial and glacial). We calculated mega-biomes from the plant-functional types (PFTs) generated by the model to allow for a direct comparison between model results and palynological vegetation reconstructions.

Our calculated mega-biomes for the pre-industrial period and the LGM corresponded well with biome reconstructions of the modern and LGM time slices, respectively, except that our pre-industrial simulation predicted the dominance of grassland in southern Europe and our LGM simulation resulted in more forest cover in tropical and sub-tropical South America.

The HE1-like simulation with a glacial climate background produced sea-surface temperature patterns and enhanced inter-hemispheric thermal gradients in accordance with the “bipolar seesaw” hypothesis. We found that the cooling of the Northern Hemisphere caused a southward shift of those PFTs that are indicative of an increased desertification and a retreat of broadleaf forests in West Africa and northern South America. The mega-biomes from our HE1

simulation agreed well with paleovegetation data from tropical Africa and northern South America. Thus, according to our model-data comparison, the reconstructed vegetation changes for the tropical regions around the Atlantic Ocean were physically consistent with the remote effects of a Heinrich event under a glacial climate background.

1 Introduction

Heinrich events (HE) are associated with abrupt climate changes (Bond et al., 1993; Broecker, 1994) and correlated with a slowdown or collapse of the Atlantic Meridional Overturning Circulation (AMOC) and a reduced formation of North Atlantic Deep Water (NADW) (e.g. Vidal et al., 1997; Cortijo et al., 1997; McManus et al., 2004). They are characterized by distinct layers of ice-rafted debris in ocean sediments, which stem from the melting of large icebergs in the North Atlantic Ocean that originated from the disintegrating Laurentide and Fennoscandian ice sheets (Bond et al., 1992, 1993; Broecker et al., 1992; Grousset et al., 2000; Hemming, 2004). Consequently, these events resulted in ice-sheet thinning and rising sea level (Yokoyama et al., 2001; Chappell, 2002; Flückiger et al., 2006). Currently, it is debated whether the iceberg discharges were the consequence or the cause of a weakened AMOC (Flückiger et al., 2006; Clark et al., 2007), although it is widely accepted that these events impacted the climate of mid- and high latitudes in the Northern Hemisphere (e.g. Schmitter et al., 2002).

The AMOC links climate change in the Northern Hemisphere with that of the Southern Hemisphere. This is

expressed in the bipolar seesaw hypothesis, whereby a cooling in the Northern Hemisphere is associated with a warming in the Southern Hemisphere (Broecker et al., 1985). Records from the Southern Hemisphere indicate a higher SST during HE1 (Lamy et al., 2007; Barker et al., 2009), while several modeling studies confirm the importance of this mechanism for regional climate changes during the glacial period (Meissner et al., 2003; Crucifix et al., 2005; Roche et al., 2007). Nevertheless, how cooling in the North Atlantic Ocean and warming in the South Atlantic Ocean during HE1 are linked to changes in the vegetation around the tropical Atlantic has not been sufficiently clarified.

Past studies focusing on processes in the mid- to high latitudes of the Northern Hemisphere successfully attributed abrupt climate change to changes in the AMOC (e.g. McManus et al., 2004). Other studies suggest that tropical regions are also affected by climate change related to HEs (Arz et al., 1998; Peterson et al., 2000; Altabet et al., 2002). Although it is probably not a driver of abrupt climate change, the tropical climate may react very sensitively to changes in the AMOC and act as an amplifier (Chiang, 2009). The climatic shifts around the tropical North Atlantic Ocean are associated with large changes in the vegetation distribution, which is likely the result of a southward shift of the tropical rainbelt, as indicated by records from the Cariaco Basin (Hughen et al., 2004; Gonzalez et al., 2008), Northeast Brazil (Behling et al., 2000; Ledru et al., 2006; Dupont et al., 2010), and North West Africa (Mulitza et al., 2008; Hessler et al., 2010). These data emphasize the importance of the tropics and the changes in tropical vegetation during periods of abrupt climate change.

By better understanding the connection between the variability of tropical vegetation and climate changes at high northern latitudes, we may enhance our ability to predict and explain the response patterns of global vegetation to abrupt climate change. Therefore, we want to examine how vegetation around the tropical Atlantic may have responded to changes in AMOC intensity during the HE1 period. Earlier model studies simulated changes during HE1 by perturbing the freshwater budget of the northern North Atlantic Ocean starting from an interglacial or glacial background climate. These studies have addressed several aspects of AMOC changes during the HE1 period such as the response time of the terrestrial biosphere (Scholze et al., 2003), the comparison between numerical model results and a pollen record from the Alboran Sea (Kageyama et al., 2005), the effect on global terrestrial carbon storage (Köhler et al., 2005), and the contribution of the terrestrial and marine carbon cycle (Menviel et al., 2008). Additionally, model studies of the HE1 period by Kageyama et al. (2005) suggest the dominance of grassland in southern Europe (the Mediterranean) due to a lower coldest-month temperature in that area; Menviel et al. (2008) found a change towards drier climate conditions in equatorial and northern South America. However, our understanding is limited of how the vegetation patterns

around the tropical Atlantic were affected during the HE1 period.

Tropical vegetation is mostly sensitive to changes in regional precipitation, which are mainly related to shifts of the Intertropical Convergence Zone (ITCZ). The position of the ITCZ over the tropical Atlantic Ocean is, in turn, linked to North Atlantic sea surface temperatures (SSTs) over the last glacial period, as suggested by several proxy studies (e.g. Peterson et al., 2000; Mulitza et al., 2008). During HE1, the northernmost position of the ITCZ likely shifted southward leading to a drier climate in West Africa and northern South America (e.g. Hughen et al., 2004; Menviel et al., 2008). However, Collins et al. (2011) suggest that the tropical rainbelt, which is associated with the yearly migration of the ITCZ, contracted rather than shifted southwards during the HE1 period.

To model the dynamic tropical vegetation response, we used an EMIC containing a Dynamic Global Vegetation Model (DGVM), i.e. the University of Victoria Earth System-Climate Model (UVic ESCM, version 2.8, cf. Weaver et al., 2001). We considered the effect of a slow-down of the AMOC for two different background climate states, corresponding to the pre-industrial and the Last Glacial Maximum (LGM, about 23 to 19 kyr BP) time periods. To simplify the comparison between the model results and paleovegetation reconstructions, we computed the biome distribution from the simulated plant-functional type (PFT) coverage and climate. Up until now, only a few studies have attempted to calculate the biome distribution (Crucifix et al., 2005; Roche et al., 2007) and none as yet has compared the model results with data from the Atlantic tropical region during HE1.

The paper is arranged accordingly. The model and biome analysis method is described in Sect. 2 together with the experimental setup. In Sects. 3 and 4, we present the results of the simulations for the pre-industrial, LGM and HE1 time periods in terms of the change in climate and biome distribution in the tropical Atlantic region, and we then compare them to paleoclimate proxies and paleovegetation records. Section 5 discusses the results, also in comparison to other Atlantic regions and in relation to the climate state background. Summary and conclusions appear in Sect. 6.

2 Methods and experimental design

2.1 The UVic ESCM and TRIFFID DGVM

The UVic ESCM incorporates an energy-moisture balance atmospheric model (Fanning and Weaver, 1996), a dynamic global vegetation model (Cox, 2001), a three dimensional ocean general circulation model (Pacanowski, 1995), and a dynamic-thermodynamic sea ice model (Hibler, 1979; Hunke and Dukowicz, 1997; Bitz et al., 2001). The model has a grid cell resolution of $3.6^\circ \times 1.8^\circ$ (longitude \times latitude)

with one vertically-averaged layer in the atmospheric model, and 19 vertical levels in the ocean model. The annual cycle of incoming solar radiation (insolation) for present and past orbital configurations is included as an external forcing factor (Berger, 1978). In addition, we use a mean-monthly wind stress climatology created from daily reanalysis data from 1958–1998 (Kalnay et al., 1996) to force the ocean and sea-ice components of the model.

The UVic ESCM also contains a land surface scheme MOSES 2 (Cox et al., 1999) and a DGVM called TRIFFID (Top-down Representation of Interactive Foliage and Flora Including Dynamics – Cox, 2001) as described by Meissner et al. (2003). The TRIFFID model calculates the plant distribution based on the CO₂ fluxes between land and atmosphere and as represented by the structure and coverage of five Plant Functional Types (PFTs) and soil carbon storage. The CO₂ flux depends on climate and the CO₂ concentration gradient between the land and atmosphere, which is calculated in MOSES 2. Any change in the CO₂ flux causes corresponding changes in PFT coverage and structure. In TRIFFID, carbon fluxes in each PFT are derived from the photosynthesis-stomatal conductance model developed by Cox et al. (1999), which utilizes an existing model of leaf-level photosynthesis in C₃ and C₄ plants (Collatz et al., 1991). In TRIFFID and MOSES 2, five PFTs (broadleaf trees, needleleaf trees, C₃ grasses, C₄ grasses, and shrubs) serve as vegetated land cover types. Non-vegetated land cover types consist of bare soil, inland water, and continental ice (Cox, 2001). To simplify the comparison of the TRIFFID output with available paleovegetation reconstructions, we developed an algorithm to compute biomes from a combination of PFTs and climate model output. For a full description, see the biome analysis Sect. 2.3.

2.2 Simulation design and boundary conditions

The control simulation (PI_CNTRL) was forced by boundary conditions characteristic of the pre-industrial period with an atmospheric CO₂ concentration of 280 ppm, a solar constant of 1365 Wm², a present-day wind field, orbital parameters from 1950 AD, and ice sheet topography and vegetation distribution from modern observations (Meissner et al., 2003), and it was integrated over a period of 2000 years to reach an (quasi-) equilibrium state. The equilibrium LGM run used the orbital parameters for 21 kyr BP, an atmospheric CO₂ concentration of 200 ppm and the ICE-5G ice-sheet reconstructions for the last glacial maximum (Peltier, 2004); it was integrated over the same period of time.

To investigate Heinrich like-climate (HE1) conditions and analyze the vegetation distribution in the tropics, we forced the UVic ESCM by adding freshwater in the North Atlantic Ocean using last glacial maximum (or glacial, HE1_GL) and pre-industrial (or interglacial, HE1_IGL) boundary conditions. The two HE1 experiments started from an equilibrium state (i.e., the HE1_GL from the LGM equilibrium

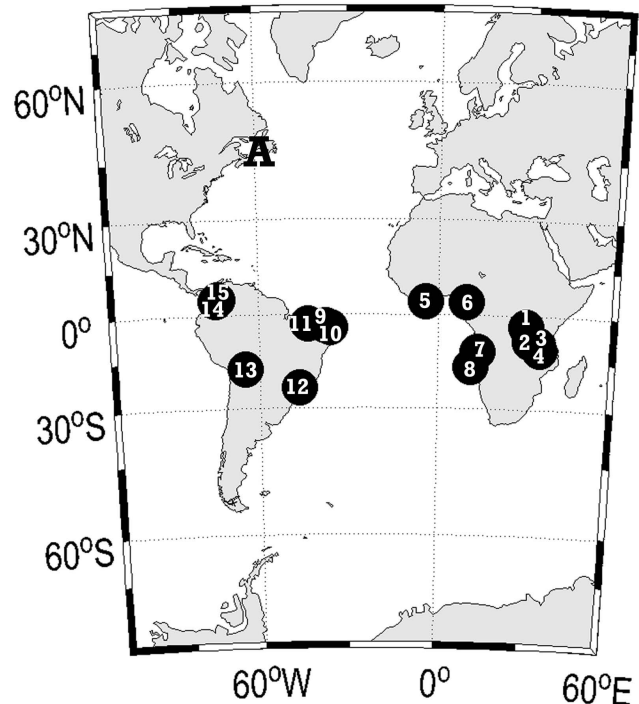


Fig. 1. Freshwater discharge location for our Heinrich Event 1 climate-like simulations (St. Lawrence River, location A) and paleovegetation proxy locations (black circles, numbers refer to the sites listed in Table 1) covering the Heinrich Event 1 period from Hessler et al. (2010) in tropical Africa and South America.

simulation, and HE1_IGL from the PI_CNTRL simulation). In each HE1 simulation, we added freshwater to the North Atlantic region at the St. Lawrence River mouth (Fig. 1 region A) during a 500 year period at a constant rate of 0.1 Sv (1 Sv = 10⁶ m³ s⁻¹) (cf. Hemming, 2004). These two HE1 simulations with two different climate backgrounds were used to reveal differences in vegetation response with respect to a reduced and a collapsed AMOC. An overview of all simulations in this paper is given in Table 1. For all analyses, we used the mean-annual results for analyzing the climate conditions and the vegetation distribution.

2.3 Biome analysis from TRIFFID

In order to compare the model output with paleovegetation reconstructions, we generated vegetation distributions in terms of biomes using the PFT coverage and temperatures from the UVic ESCM output. The simulated atmospheric temperature was used to calculate the parameters constraining biomes, such as temperature of the coldest month (T_c), temperature of the warmest month (T_w), and the number of growing degree-days above 0 °C and 5 °C (GDD0 and GDD5, respectively). These constraints were chosen based on the definition of biomes in the BIOME 4 model (Kaplan et al., 2003).

Table 1. Boundary conditions (including atmospheric CO₂ in atmosphere, amount and location for freshwater perturbation) and simulation design for all simulations analysed in the present paper.

Simulation	Orbital parameter	CO ₂ concentration	Freshwater anomaly		Years simulation
			amount (Sv)	Location	
Equilibrium					
PI_CNTRL	Pre-industrial	280			2000
LGM	21 kyr BP	200			2000
Heinrich event					
HE1_I_GL	Pre-industrial	280	0.1	A	500
HE1_GL	21 kyr BP	200	0.1	A	500

Table 2. Distribution of dominant PFTs based on the percentage of PFT coverage.

Dominant PFTs or PFTs mixture	PFT coverage
	BL, NL, SH, C ₃ , C ₄ over 50 %
Broadleaved trees (BL)	BL ≥ 50 %
Needleleaved trees (NL)	NL ≥ 50 %
Shrubs (SH)	SH ≥ 50 %
C ₃ grass (C ₃)	C ₃ ≥ 50 %
C ₄ grass (C ₄)	C ₄ ≥ 50 %
	BL, NL, SH, C ₃ , C ₄ less than 50 %
Mixed trees	BL + NL ≥ 50 %
Mixed vegetation (without trees)	SH + C ₃ + C ₄ ≥ 50 %
Open vegetation	20 % ≤ BL + NL + SH + C ₃ + C ₄ ≤ 50 %
Barren soil	BL + NL + SH + C ₃ + C ₄ < 20 %

The dominant PFT in each grid cell is evaluated based on the percentage of PFT coverage. If the percentage of PFT coverage is over 50 %, the PFT potential is set equal to the dominant PFT (broadleaved trees, needleleaved trees, shrubs, C₃ grass, or C₄ grass). If it is less than 50 %, the grid cell is designated as mixed trees if it is dominated by tree PFTs, as mixed vegetation if non-trees PFTs are dominant, as open vegetation if all PFTs are between 20 % and 50 %, and as desert if all PFTs together are less than 20 % (Crucifix et al., 2005).

To attain the biome distribution, we calculated the potential PFT coverage for each grid cell based on the fractional PFT coverage (Table 2; Crucifix et al., 2005), and then combined both the environmental limitation and the potential PFTs (Table 3; Prentice et al., 1992; Harrison and Prentice, 2003; Roche et al., 2007). By a “potential PFT”, we mean either the dominant PFT or a mixture of PFTs in each grid cell, which we calculated based on the percentage of PFT coverage. We finally compared the biome distribution based on the model output with biome distributions derived from paleovegetation reconstructions. To simplify the comparison, we used nine biomes which are classified as

the “mega-biomes” in BIOME 6000 (Harrison and Prentice, 2003), and the global data sets from Prentice et al. (2000), Harrison et al. (2001), Bigelow et al. (2003), and Pickett et al. (2004) (see also http://www.bridge.bris.ac.uk/resources/Databases/BIOMES_data). The nine biomes included are tropical forest, warm-temperate or mixed forest, temperate-montane forest, boreal forest, savanna and dry woodland, grassland and dry shrub land, desert, dry tundra, and tundra.

3 The equilibrium simulations

Our equilibrium simulations PI_CNTRL and LGM represent two background climate states of the Earth system corresponding to pre-industrial and LGM boundary conditions, respectively. Generally the UVic ESCM reaches a near-equilibrium state after about 2000 years of integration; by that time the annually-averaged surface fluxes are close to zero (Weaver et al., 2001).

3.1 Pre-industrial simulation (PI_CNTRL)

The equilibrium climate conditions resulting from the pre-industrial control simulation (PI_CNTRL) are summarized in Fig. 2. The simulated SSTs (Fig. 2b) are in general agreement with the World Ocean Atlas (Conkright et al., 1998). However, there is a cold bias in the tropical Atlantic Ocean, a warm bias along the mid-latitude Atlantic coasts (e.g. the west coast of southern Africa and east coast of North America), and a cold bias in the Gulf of Alaska and the Greenland, Iceland and Norwegian seas (cf. Weaver et al., 2001). Tropical (between 30° N to 30° S) annual mean precipitation simulated in PI_CNTRL ranged from 0.1 m yr⁻¹ to 2.5 m yr⁻¹ (Fig. 2c). Low precipitation values (below 0.5 m yr⁻¹) occurred in southern Africa and southern South America, in the high latitudes in both hemispheres, and in northern subtropical Africa. High terrestrial precipitation (above 1.5 m yr⁻¹) occurred in northern South America, central North America and central Africa, while oceanic precipitation was highest

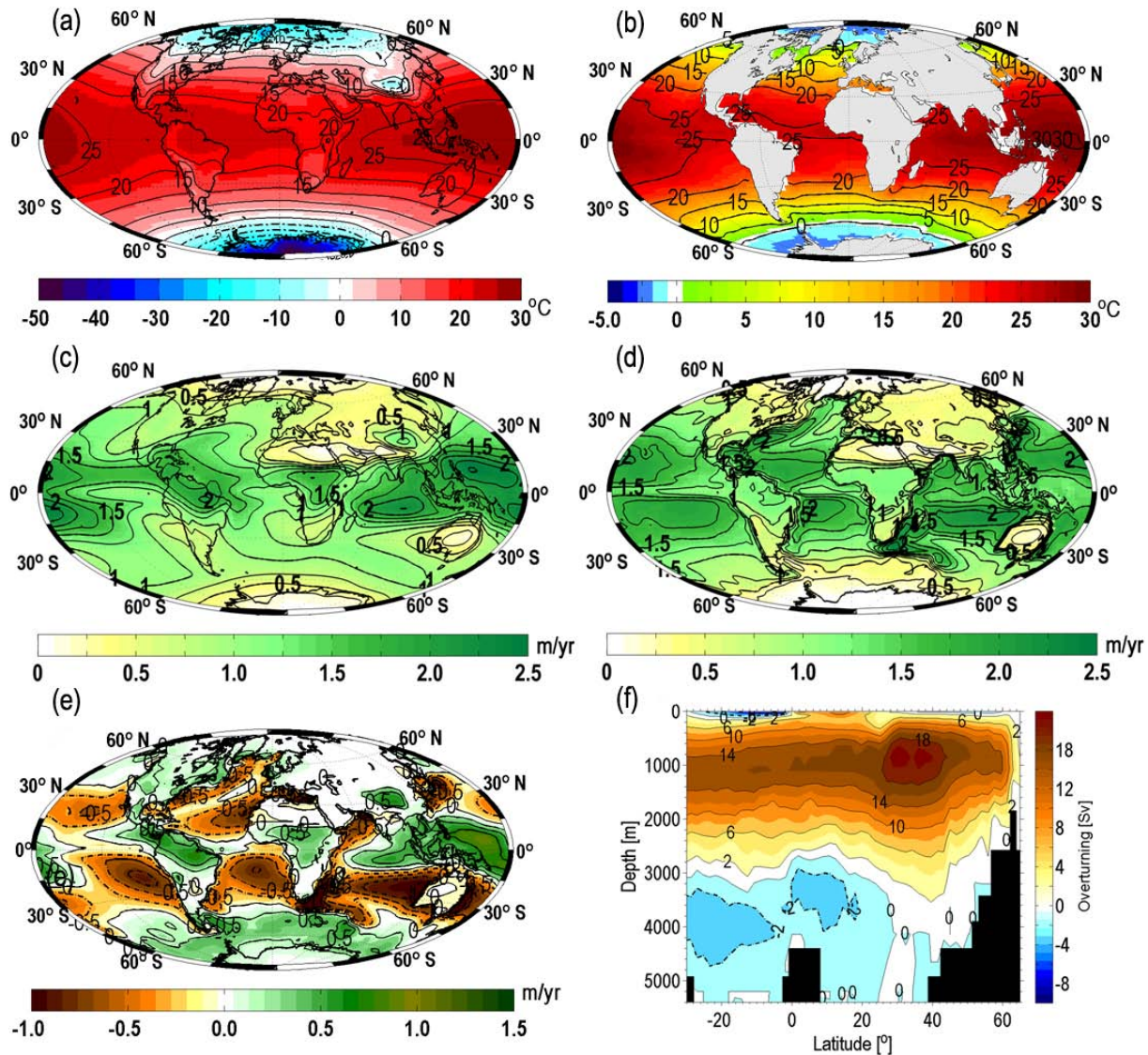


Fig. 2. Annual-mean of (a) surface air temperature (SAT), (b) sea surface temperature (SST), (c) precipitation, (d) evaporation, (e) precipitation minus evaporation ($P - E$), and (f) zonally integrated meridional overturning streamfunction in the North Atlantic for the pre-industrial simulation (PI_CNTRL). Contour intervals in SAT and SST are 5°C . Contour intervals of the streamfunction of AMOC formation is 4 Sv ($1\text{ Sv} = 10^6\text{ m}^3\text{ s}^{-1}$). Solid line contours indicate a clockwise circulation while dotted lines denote a counterclockwise circulation.

(above 2.0 m yr^{-1}) over the equatorial East Pacific and Indian Oceans. Although the simulated precipitation patterns are similar to the NCEP/NCAR reanalysis data (Kalnay et al., 1996; Weaver et al., 2001) (e.g. both data and model have high precipitation in northern South America and central Africa), there are differences in position or intensity. For example, the simulated precipitation in northern South America is less intense than observed. The maximum of precipitation was simulated over the western Pacific Ocean, while the data shows it in northwestern South America.

The evaporative loss over the oceans simulated in PI_CNTRL reached approximately 1.5 to 2.0 m yr^{-1} , and in some cases more than 2.0 m yr^{-1} (Fig. 2d). Evaporation in northern and southern high latitudes, as well as in subtropical

regions such as northern Africa, the Middle East, and Australia, was relatively low (below 0.4 m yr^{-1}). In northern South America and central Africa, the evaporative loss from land was estimated at about 1.0 m yr^{-1} , which was less than over the adjacent North or South Atlantic Oceans. These patterns in the PI_CNTRL simulation correspond well to the NCEP/NCAR data, which also show low evaporation rates in northern Africa and Australia and high evaporation rates in northern South America and central Africa. Our simulation compares better to observations than the present-day simulation by Weaver et al. (2001), possibly because our version of the UVic ESCM includes a DGVM that leads to a more realistic representation of the hydrological cycle.

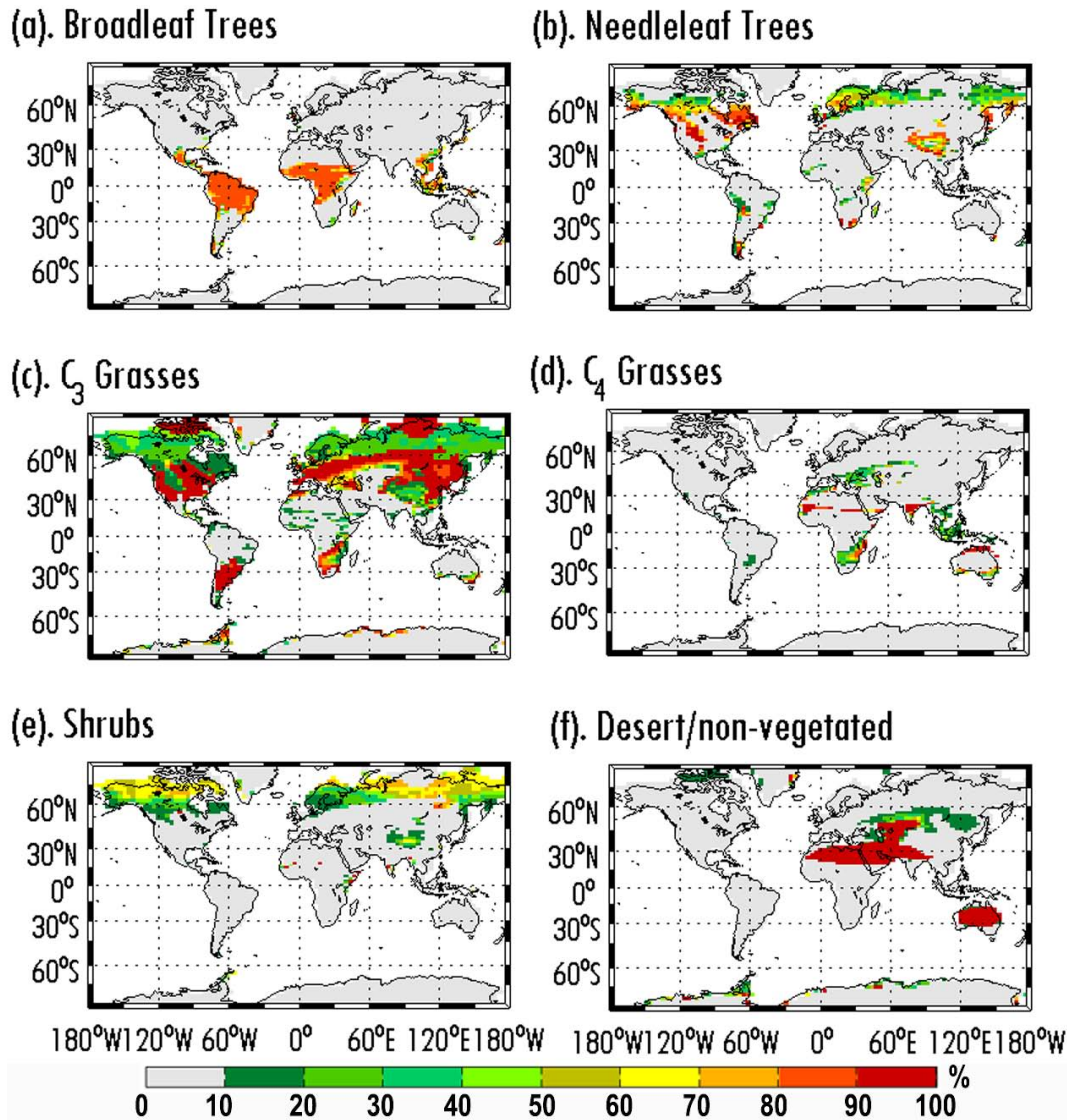


Fig. 3. Annual-mean of plant functional type (PFT) covers for: (a) broadleaf trees, (b) needleleaf trees, (d) C_3 grass, (d) C_4 grass, (e) shrubs, and bare soil coverage (f) desert/not vegetated for the PLCNTRL simulation.

The PLCNTRL simulation also indicated a net gain of freshwater in northeast and southern South America as well as in central Africa (Fig. 2e). A net gain of freshwater corresponds to more precipitation than evaporation, leading to better conditions for a more robust tree cover (e.g. tropical forest). The zonally integrated meridional overturning circulation in the Atlantic Ocean (AMOC) for the PLCNTRL simulation indicates a North Atlantic Deep Water (NADW) cell and an Antarctic Bottom Water (AABW) cell (Fig. 2f). This pattern is typical of an active mode of the Atlantic thermohaline circulation under conditions similar to the present day. The maximum of the streamfunction was 21 Sv and found between 35° and 40° N at 1000 m depth. The export of NADW across the equator into the South Atlantic Ocean was about 14 Sv, which is comparable to observations

(for example, Lumpkin and Speer, 2007, give a value of 17.9 ± 3.1 Sv). The AABW that originated from the Southern Ocean flowed across the equator into North Atlantic Ocean at a rate of 2 Sv and penetrated as far north as about 20° N.

The vegetation cover in the UVic ESCM is represented by PFTs, which in our study were used to calculate the biome distribution. Figure 3 shows the annual-mean PFT distribution for the PLCNTRL simulation as a fraction of the area covered in each grid cell of the model. Broadleaf trees were dominant in the tropics (e.g. in South America, Africa, and the Indo-Pacific region between 15° N to 15° S). Needleleaf trees were dominant in northern high latitudes such as northern Siberia and North America, but also at high elevation in northern India (Himalayan Mountains), where the

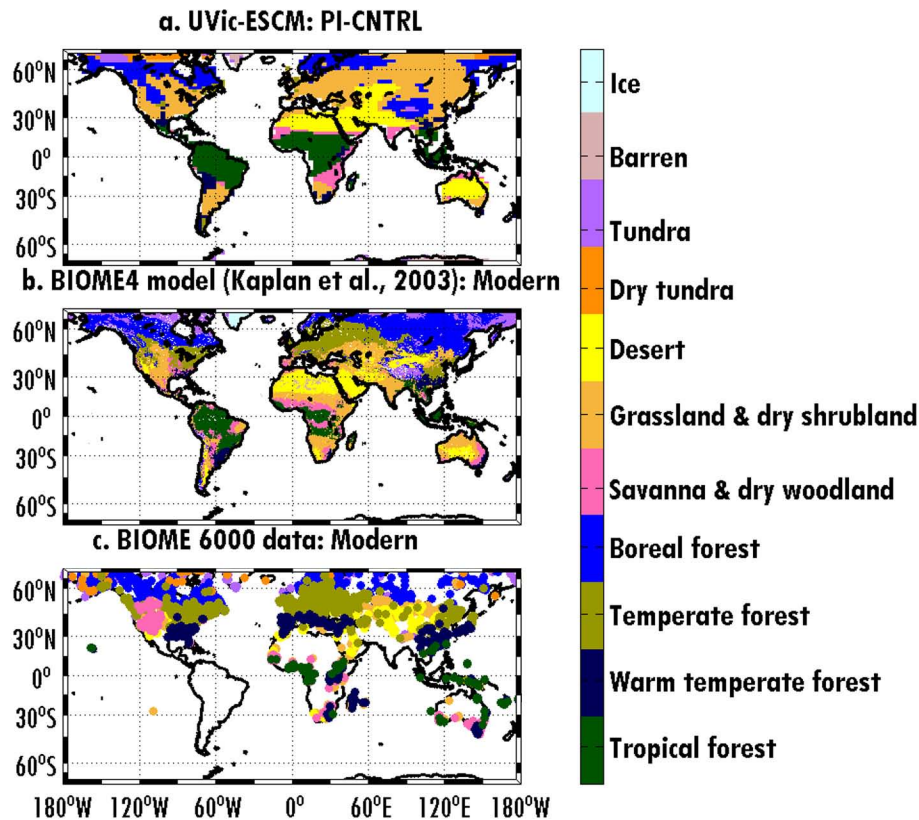


Fig. 4. Mega-biome distribution for (a) PI-CNTRL biomes simulated in UVic ESCM, (b) modern biomes by the BIOME 4 (Kaplan et al., 2003), and mapping of modern pollen samples by BIOME 6000 (Prentice and Webb, 1998). The UVic ESCM biomes are computed as a combination of environmental constraints and potential PFTs, and the mega-biomes are defined after Harrison and Prentice (2003).

fractional cover is between 40 to 90%. The C₃ grasses covered a large area of the globe and reached high percentages in northern Eurasia and North America. The C₄ grasses were simulated in Southeast Africa with low percentages (around 10%), while a coverage of more than 80% was reached in North Africa, northern India, and Australia. This type of grasses is better adapted to a dry and hot climate, while the C₃ grasses grow preferentially in a cooler and wetter climate. Shrubs are also representative of a cooler climate and occur together with needleleaf trees in northern Siberia and North America. Our results mostly agree with the PFT distribution simulated by Meissner et al. (2003), except that they obtain more broadleaf trees in Central America and a higher percentage (mostly above 60%) of needleleaf trees at the northern high latitudes.

The biome distribution is plotted in Fig. 4. A high fractional coverage of tropical forest is shown in northern South America in areas such as the Amazon rain forest, northern Brazil, Venezuela, Colombia, and Peru. The tropical forest cover, represented by the broadleaf trees PFT in the model, was similar to results by Meissner et al. (2003) and Crucifix et al. (2005). However, our model simulated tropical forest in northern Venezuela and Northeast Brazil, whereas today

these regions are covered by savannah, grassland, and shrubland as shown by the BIOME 4 model (Kaplan et al., 2003; Fig. 4b).

In our control simulation, tropical North America was dominated by tropical forest, although we find small areas of savannah in Central America. This biome pattern agrees with Kaplan et al. (2003), who obtain tropical forest, savannah, and temperate forest in this region, and it is also similar to the findings by Crucifix et al. (2005) and Meissner et al. (2003), who predict a dominance of tropical forest biomes over broadleaf forest cover. Sub-tropical North America was estimated to be dominated mostly by grassland while small areas of boreal and temperate forests were found in central North America. However, a different distribution is reported by Crucifix et al. (2005), Meissner et al. (2003) and Kaplan et al. (2003) who estimate a dominance of temperate and boreal forest, and also regionally of desert and grassland. Observations made by Loveland et al. (2000) and the BIOME 6000 project (Fig. 4c) conclude that the area is dominated by open shrubland or savannah in western North America, grasslands in the central region, and mixed boreal and temperate forest in eastern North America. Thus our model did not reproduce the observed vegetation distribution in North America,

Table 3. Environmental constraints and potential PFTs used to compute the biome distribution from UVic ESCM results.

Biome	Dominant PFTs or PFTs mixture	Environmental Constraint				
		T_c	GDD5	GDD0	T_w	
		min	min	min	min	max
Tropical forest	BL trees	15.5				
Warm-temperate forest	BL trees or mixed trees	5				
Temperate forest	BL trees or NL trees or mixed trees	-2				
Boreal forest	BL trees or NL trees or mixed trees	-32.5				
Savanna and dry woodland	Grass or mixed vegetation or open vegetation	17				
Grassland and dry shrubland	Grass or mixed vegetation or open vegetation		500		10	
Desert	Barren soil				22	
Dry tundra	SH or mixed vegetation					15
Tundra	SH or mixed vegetation			800		15

The land temperatures from the UVic ESCM are used to calculate the temperature of the coldest month (T_c), growing degree-days relative to 5 °C and 0 °C (GDD5 and GDD0), and temperature of the warmest month (T_w) following BIOME 4 (Kaplan et al., 2003). The assignment of a particular biome to a grid cell is based on the BIOME 6000 project version 4.2 after Prentice et al. (1992), Harrison and Prentice (2003), and Roche et al. (2007).

neither regarding location nor in terms of the general pattern. The discrepancy is likely due to an overestimation of C_3 grasses precluding the simulation of dominant tree cover and hence, the formation of mixed boreal and temperate forest mega-biomes.

In experiment PL_CNTRL, we simulated tropical forests in western and central Africa between 20° N and 20° S. In the Sahel region and along the east coast of Africa, the biome distribution was mostly savannah, while to the south mixed grassland and warm temperate forest prevailed. These patterns generally agree with both the BIOME 4 model and BIOME 6000 data (Fig. 4b and c). The BIOME 4 model estimates grassland and savannah in the Sahel, tropical forest along the west coast and extending into central Africa (Angola, Congo, and Zambia), and grasslands in eastern Africa. The BIOME 6000 data shows mostly tropical forest in western equatorial Africa, and grassland and savannah in the Sahel. Our model failed to simulate desert and savannah at the southern tip of Africa, where the BIOME 4 model and BIOME 6000 data show a mix of savannah, desert, warm-temperate forest, and grassland. Another discrepancy occurs in southern Europe, where the biomes estimated in the PL_CNTRL simulation did not reveal a warm-temperate forest as evidenced by data from the BIOME 6000 project. It seems that our model overestimated the growth of C_3 grasses in those areas, and hence Europe and Eurasia were covered by the grassland biome in our simulation.

3.2 Last Glacial Maximum simulation (LGM)

The LGM experiment simulated cooler surface air temperatures (SATs) and SSTs than the PL_CNTRL (Fig. 5a and b). The largest SAT cooling occurred near the ice sheets (up to -20 °C and -40 °C different from PL_CNTRL in North

America and Antarctica, respectively). However, there was also a moderate cooling of SAT in the tropics (Fig. 5a) where differences between LGM and PL_CNTRL were around 3 °C. The largest SST anomaly occurred in the western North Atlantic Ocean where the differences between LGM and PL_CNTRL reached more than 9 °C, while the cooling in the tropics amounted to 3 and 2 °C (Fig. 5b). The LGM precipitation patterns were overall similar to PL_CNTRL, except that the intensity was reduced by 0.3 to 0.5 m yr⁻¹ (Fig. 5c). As in the PL_CNTRL simulation, the AMOC in the LGM simulation (Fig. 5d) was also in the active mode. The maximum of the meridional overturning streamfunction was 7 Sv less than in the PL_CNTRL simulation (13.5 Sv as compared to 21 Sv), located further south and at a slightly shallower depth (~100 m less). NADW was transported across the equator and exported to the South Atlantic Ocean at a rate reduced by about 40 % (from 14 Sv to 8 Sv), while the inflow of AABW from the South Atlantic Ocean was similar (2 Sv) but reached further northward (up to 25° N) to replace part of the NADW.

Differences between the LGM and the PL_CNTRL biomes were most pronounced in northern and eastern Africa and western South America (Fig. 6a), where drier biomes were predicted for the LGM. Otherwise, our LGM results were similar to those of our PL_CNTRL simulation (Figs. 4a and 6a), especially in northern South America (tropical forest) and southern South America (grassland and dry-shrubland), although we found a few locations in South America where the biome distribution was different. In western South America, warm-temperate forest changed to boreal forest, and warm-temperate forest extended from middle and eastern Brazil to western Brazil, indicating reduced temperature and precipitation that affected the PFT coverage in the LGM simulation. The LGM simulation also indicated drier conditions in southeast South America by the presence of

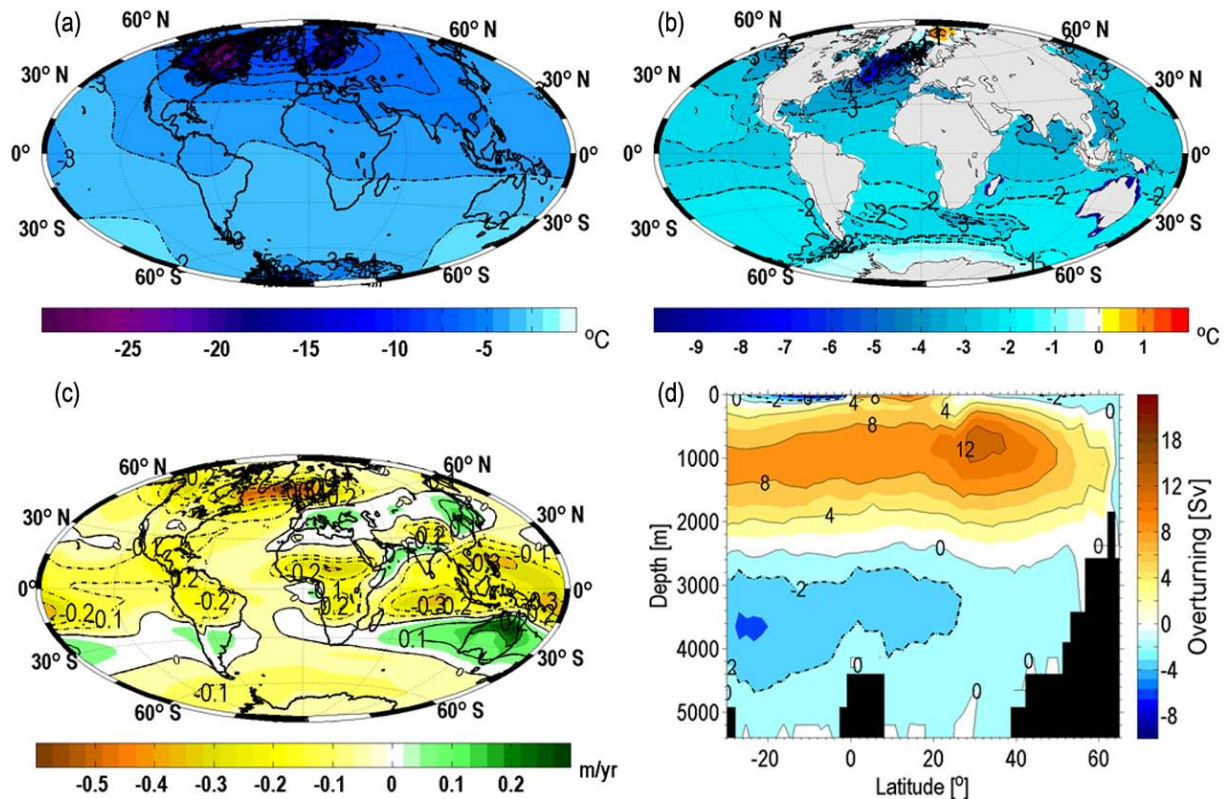


Fig. 5. Annual-mean anomaly showing differences between the LGM and the PL_CNTRL simulations for: (a) surface air temperature (SAT), (b) sea surface temperature (SST), (c) precipitation, and (d) the zonally integrated meridional overturning streamfunction (Sv) in the North Atlantic for the LGM simulation with a fixed volume contour interval of 4 Sv similar as Fig. 2f. Contour intervals for SAT and SST are 1 °C.

grasslands and shrublands. Our results generally agree with the LGM simulations by Crucifix et al. (2005) and Henrot et al. (2009), which show a dominance of open vegetation and C₃ grasses. Paleovegetation reconstructions from plant fossil and proxy data sources such as in Ray and Adams (2001) also suggest drier conditions in these areas which are dominated by desert and semi-desert.

In central North America temperate forest was partly replaced by boreal forest. The vegetation in our LGM simulation showed a similar bias in North America as the PL_CNTRL simulation. The C₃ grass cover was overestimated in comparison to other simulations (e.g. Crucifix et al., 2005; Roche et al., 2007), which predict a dominance of cool forest biomes such as needleleaf, mixed and temperate broadleaf forests, even though they also simulate warm grasses and savannah in eastern regions and tropical forest in western regions. Similarly, the BIOME 6000 project reconstructions predict boreal and temperate forest in eastern North America and a dominance of savannah in western North America. All models seem to be consistent with the proxy data that indicate the presence of vegetation adapted to cooler conditions during the LGM compared to the present day, although the location and biome types do not exactly match those of the vegetation reconstructions.

Our LGM simulation yielded warm-temperate forest and grassland in the Sahel region in contrast to tropical forest and savannah in the PL_CNTRL simulation. The LGM tropical forest cover showed a similar pattern but with lower percentages than in the PL_CNTRL simulation. A decrease of tropical forest in central Africa is consistent with a lower temperature and reduced precipitation during the LGM (Figs. 2 and 5). This pattern agrees with reconstructions by Ray and Adams (2001) and Dupont et al. (2000), who found a reduction in tropical forest in western and central Africa during the LGM period. Our model also agrees with pollen data from BIOME 6000 which show tropical forest on the west coast of Africa and grasslands in southern and northern Africa.

Both equilibrium climate simulations PL_CNTRL and LGM predicted similar dominant biomes in the Indonesian Archipelago (tropical forest) and in Australia (savannah, grassland, and desert). The difference in biomes between the pre-industrial and LGM simulations is only through a reduction in vegetation cover, where savannah in northern Australia and grasslands in southern Australia were replaced by desert. Our results for southern Australia were consistent with the LGM simulation by Roche et al. (2007) and are supported by proxy data (Harrison and Prentice, 2003).

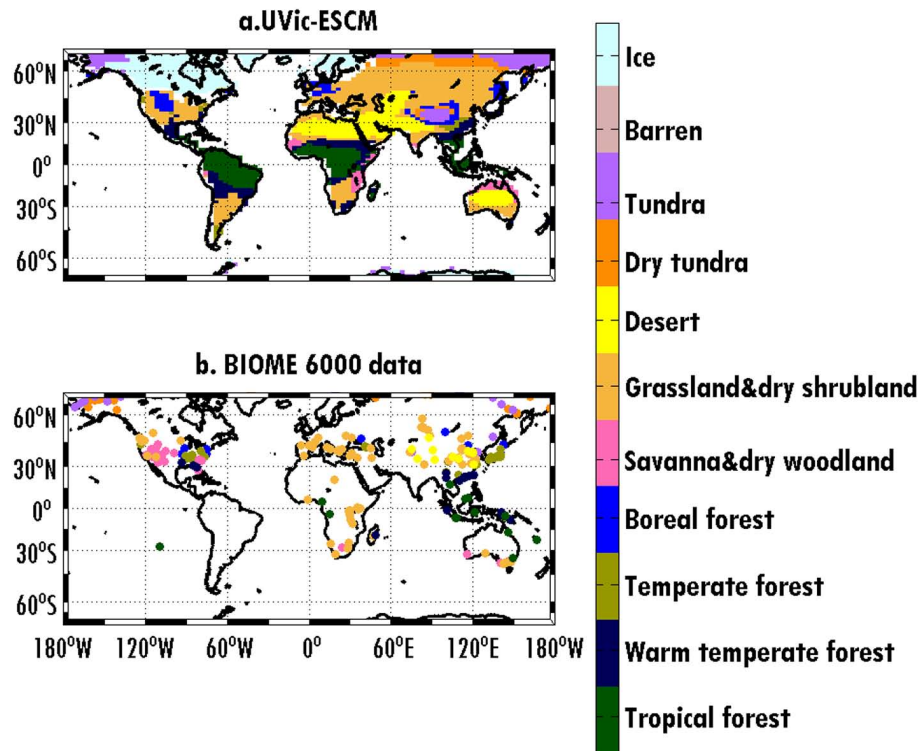


Fig. 6. Mega-biome distribution for the last glacial maximum (LGM, 21 kyr BP): (a) LGM biomes simulated by the UVic ESCM, (b) paleovegetation mapping by BIOME 6000 (Prentice and Webb, 1998).

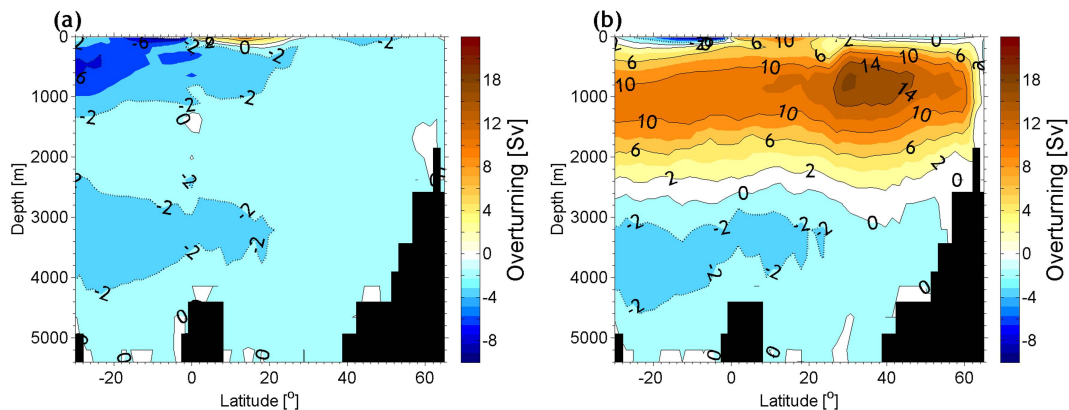


Fig. 7. Zonally integrated meridional overturning streamfunction (Sv) in the North Atlantic after 500 yr of (a) HE1_GL and (b) HE1_IJL simulations. Contour interval is a fixed volume of 4 Sv ($1 \text{ Sv} = 10^6 \text{ m}^3 \text{ s}^{-1}$). Solid line contours indicate a clockwise circulation and dotted line contours denote a counterclockwise circulation.

4 Heinrich Events 1 simulations

4.1 Changes in climate

Our HE1 simulations corresponded to a $1.6 \times 10^6 \text{ km}^3$ release of freshwater and an associated global sea level rise of 4.5 m after 500 years. This amount of water was enough to cause cessation of NADW formation in the HE1_GL

simulation, while in the HE1_IJL simulation it was only reduced from 21 Sv to 16 Sv (Fig. 7). Correspondingly, the surface salinity in the North Atlantic Ocean was strongly reduced by up to 5 psu in the HE1_GL simulation (in particular near the St. Lawrence River mouth and off western Europe and northwest Africa), while the surface salinity in the HE1_IJL simulation was only reduced by 0.5 psu. In the South Atlantic Ocean, the strongest sea surface salinity

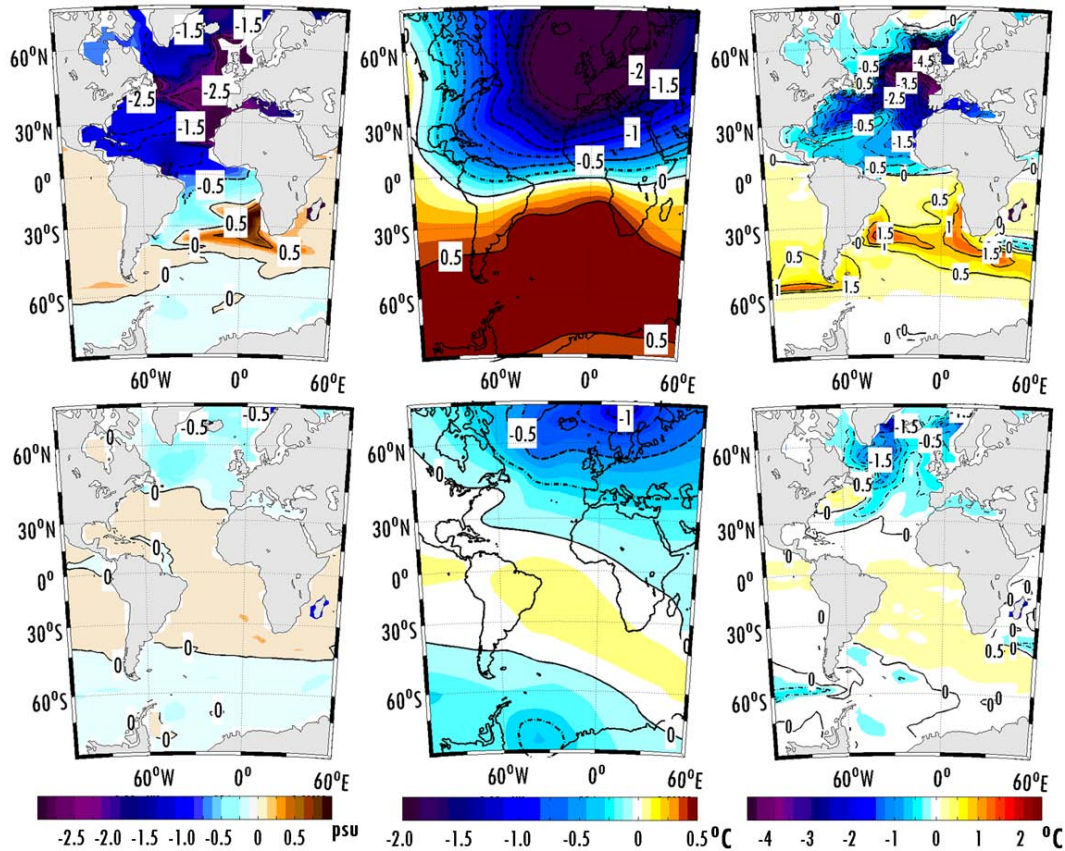


Fig. 8. Annual-mean anomaly showing differences between the HE1.GL and the LGM simulations (top panel) and the HE1.IGL and the PI_CNTRL simulations (bottom panel) for sea surface salinity (SSS, left panel), surface air temperature (SAT, middle panel), sea surface temperature (SST, right panel).

(SSS) anomaly of up to 1 psu occurred off Southwest Africa (Fig. 8, left panels). These findings are consistent with other studies examining changes in AMOC strength after adding freshwater to the Northern Hemisphere to imitate the HE1 period and showing either a decrease in the AMOC strength (Weaver et al., 2003) or a complete collapse (Menviel et al., 2008; Köhler et al., 2005) followed by a cooling of the North Atlantic Ocean during HE1.

The HE1 simulations were characterized by cooling over the northern North Atlantic Ocean (Fig. 8, middle panels). This cooling was most pronounced in the HE1.GL simulation with SAT anomalies below -2.7°C , (Fig. 8, top middle panel) while in the HE1.IGL simulation the largest negative anomaly was only around -0.5°C (Fig. 8, bottom middle). Our HE1.GL anomaly is consistent with Menviel et al. (2008) and Kageyama et al. (2010), who also found a stronger North Atlantic cooling in their HE1 simulation using a glacial climate background state instead of an interglacial one. Furthermore, slightly warmer SATs were found in the Southern Hemisphere and the North Pacific region, with maximum positive anomalies in the HE1.GL simulation exceeding 0.6°C . The largest positive anomalies in the

HE1.IGL simulation were only around 0.3°C , and occurred over the tropical Indo-Pacific Ocean (southern India, northern Australia, and southeast Asia).

The SST anomalies of the HE1 simulations reflect the bipolar seesaw effect in the North and South Atlantic Oceans (Fig. 8, right panels), which in turn is connected to precipitation changes in the tropics. The largest negative SST anomaly occurred in the eastern North Atlantic Ocean and reached around -4°C in the HE1.GL simulation (Fig. 8, top right panel). The largest positive SST anomaly (above 1.8°C) appeared along the west coast of southern Africa and at the high latitudes of the South Atlantic Ocean.

The precipitation response was strong in the HE1.GL simulation (Fig. 9, top left panel), while it was negligible in the HE1.IGL simulation (Fig. 9, bottom left panel). Precipitation decreased in the Sahel region, the Middle East, Europe and around the Gulf of Mexico, with maximum negative precipitation anomalies of -0.2 m yr^{-1} . Precipitation increased in Southwest Africa (Angola and Namibia) and southeast Argentina, with maximum positive anomalies exceeding 0.16 m yr^{-1} . In contrast, in the HE1.IGL simulation estimated anomalies were between -0.02 m yr^{-1} and

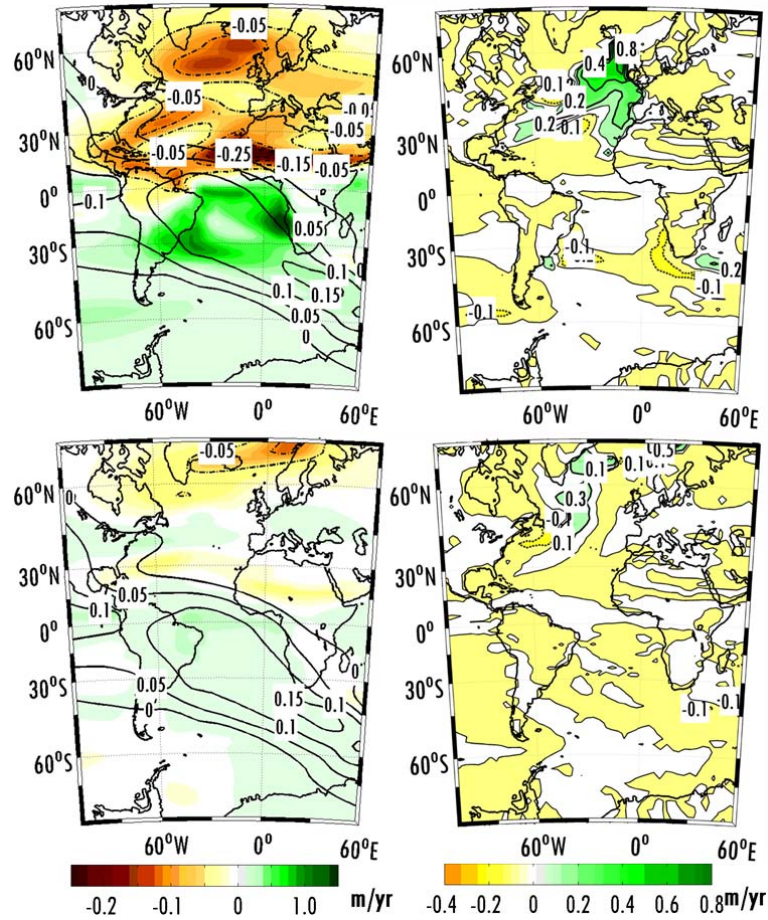


Fig. 9. Annual-mean anomaly showing differences between the HE1_GL and the LGM simulations (top panel) and the HE1_IGL and the PI_CNTRL simulations (bottom panel) for precipitation (left panel), and net flux freshwater (precipitation – evaporation – runoff, $P - E - R$, right panel).

+0.02 m yr⁻¹, only. A similar anomaly pattern is also found in other studies (e.g. Köhler et al., 2005; Menviel et al., 2008; Kageyama et al., 2010), in which it is attributed to a southward shift of the ITCZ. Due to the simplicity of the wind scheme in our atmospheric model the precipitation anomaly in our HE1_GL did not show a southward shift of ITCZ.

The net surface freshwater flux (precipitation minus evaporation minus runoff) anomaly between the HE1_GL and the LGM simulations over the Atlantic Ocean suggests that most of the North Atlantic Ocean gained more freshwater than it received. The opposite pattern is found in the northern and southern subtropical Atlantic Ocean, while the net surface freshwater flux remained nearly the same in the tropical Atlantic Ocean (Fig. 9, top right panel). The net surface freshwater flux anomaly under pre-industrial boundary conditions (Fig. 9, bottom right panel) had a pattern similar to the one under LGM boundary conditions, except that the intensity was reduced due to different responses to the freshwater perturbation in the two climate states.

The slowdown of the AMOC and reduced deepwater formation in the HE1 simulations (Fig. 7) were associated with a seesaw pattern in temperature and precipitation at the sea surface (Figs. 8 and 9). The freshwater discharges to the North Atlantic Ocean changed the density of surface water, prevented the NADW from sinking, and resulted in a reduction or shutdown of deepwater formation. The meridional overturning streamfunction shows that the formation of NADW collapsed in the HE1_GL simulation (Fig. 7a) and that AAIW (Antarctic Intermediate Water) became the dominant water mass, spreading further north until 20° N. The streamfunction in the HE1_IGL simulation (Fig. 7b) is similar to that of the PI_CNTRL simulation (Fig. 2f), except that the maximum strength was reduced from 21 Sv to 16 Sv. The weak AMOC response in HE1_IGL corresponds to weak changes in SST and precipitation.

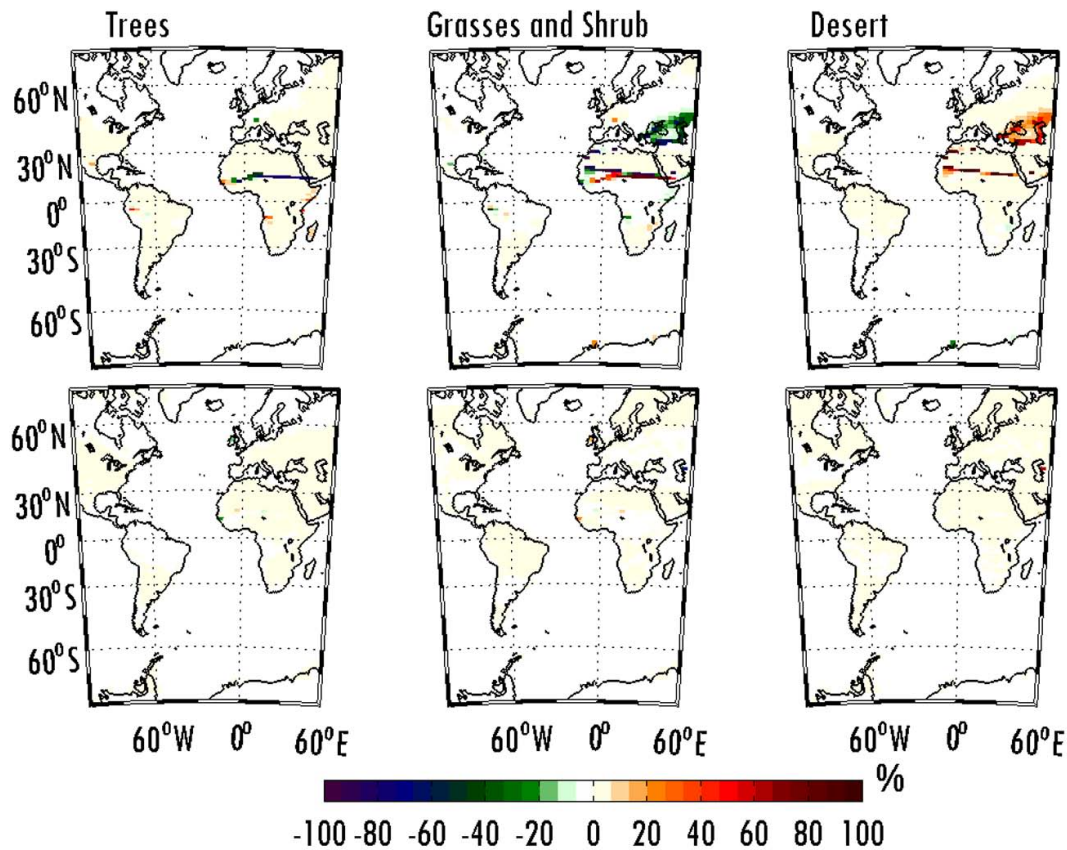


Fig. 10. Annual-mean PFT differences in percent coverage between HE1_GL and LGM (top panel) and HE1_GL and PI_CNTRL (below) for trees (left panel), grasses and shrubs (middle panel), and desert, non-vegetated coverage (right panel).

4.2 Changes in vegetation

The HE1_GL simulation showed a much more pronounced vegetation change than the HE1_IJGL simulation (Fig. 10). This is most evident in northern Africa (Sahel region) and western Asia (near present-day East Kazakhstan). These changes corresponded to changes in climate, as for example in the Sahel region, where precipitation was reduced by 0.2 m yr^{-1} in the HE1_GL simulation as compared to the LGM equilibrium simulation (Fig. 9, top left panel). This resulted in a change in PFT coverage from robust broadleaf and needleleaf forest to grassland and shrubland cover (tree cover was reduced by more than 60%). In other parts of the Sahel, grass and shrub covers decreased by more than 60% and were replaced by desert. These vegetation changes, from forest to grass and shrubs, and from grass and shrubs to desert, indicate a drier climate in the HE1 simulation than in the LGM equilibrium simulation.

South of the equator, the vegetation response in the HE1_GL simulation corresponding to a slight warming was not as robust as north of the equator. For example, in southwestern Africa precipitation increased regionally, consequently broadleaf trees cover increased by 49%, while

at the same time grass and shrub cover decreased by 51% (Fig. 10). In the HE1_IJGL simulation, changes were much smaller or even insignificant (increase or decrease are less than 10%). Grass and shrub cover in northern tropical and sub-tropical regions (0 to 30° N) in the HE1_GL simulation went almost unchanged, except for a small region in West Africa, where grasses increased by around 20% and consequently trees decreased by a similar amount. Both HE1 simulations indicated cooler and drier climatic conditions around the North Atlantic Ocean and a succession in vegetation cover in northern Africa from forest to grassland and from shrub to desert. Over the South Atlantic region, the HE1 simulations resulted in warmer and wetter climatic conditions in parallel with a regional increase of tropical forest cover in Southwest Africa. However, the increase in precipitation in South America in the HE1 simulations did not cause any change in vegetation cover compared to the equilibrium simulations. The vegetation response in Southwest Africa generally agrees with Menviel et al. (2008) who found that a wetter climate in the Southern Hemisphere did not lead to large changes in land carbon storage, and resulted in less forest cover in the Southern Hemisphere except for Southwest Africa and western South America.

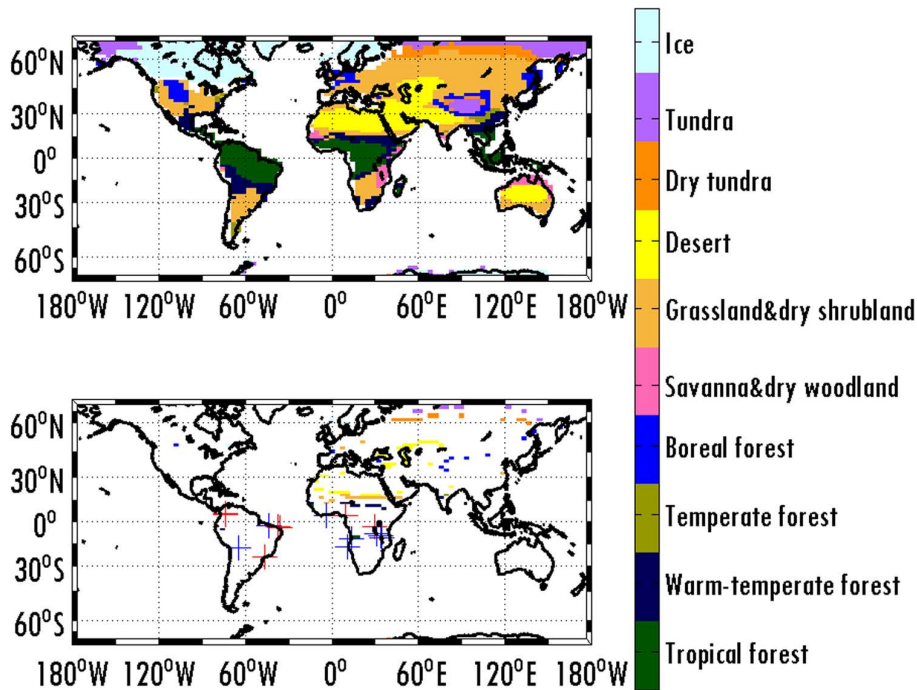


Fig. 11. Mega-biome distribution computed from UVic ESCM results; (top panel) HE1_GL simulation and (bottom panel) anomaly between HE1_GL and LGM simulations. The anomaly map shows the HE1_GL biome only in those grid cells that differ from the LGM simulation. Blue crosses indicate locations where biomes are similar in the model and the data reconstruction (Hessler et al., 2010); red crosses denote where modeled and reconstructed biomes differ.

4.3 Biome distribution and model-data comparison

To compare the HE1 simulations with vegetation proxies, we focus on the discussion of vegetation changes in the HE1_GL simulation. The biome distribution diagnosed from our HE1_GL simulation is compared with pollen records from tropical Africa and South America (Fig. 11 and Table 4, Hessler et al., 2010). Both the climate and the biome distribution exhibited a shift towards drier conditions in tropical Africa, while wetter conditions existed in South America and southern tropical Africa. The tropical African biomes (not including the Sahel) were dominated by tropical forest from western to central Africa (e.g. Gabon, Congo, Cameroon, Nigeria, Zaire, and Burundi), while in the East (e.g. Tanzania and Kenya) a mix of warm temperate, boreal forest, and savannah was simulated (Fig. 11), in accordance with a wetter climate. Even when the differences in climate were not pronounced, e.g. between West and East Africa, distinctly different biomes were established. The simulated tropical African vegetation generally agrees with several palynological vegetation reconstructions for West and East Africa (Hessler et al., 2010; Kageyama et al., 2005). However, in Burundi (central Africa), proxy records indicate a cool and dry climate dominated by grassland and savannah, while our model predicted tropical forest (Table 4). Furthermore, these records indicate that northern tropical Africa (i.e. the Sahel region) experienced drier conditions suggesting that

the biomes changed from grasslands to desert in the eastern Sahel, warm-temperate forest to grasslands in the western Sahel, and tropical forest to warm-temperate forest in the central Sahel. This supports our model result in that due to changes in climate the PFT cover in the Sahel region changed from forests to grasses or from shrubs to desert.

The changes in biome distribution of the HE1_GL simulation in northern and southern subtropical Africa show opposing trends towards drier biomes in the north and wetter biomes in the south, but the change south of the equator is far smaller than north of it. In northern subtropical and equatorial Africa our model suggested a drier climate and, accordingly, desert cover expanded in these regions. Furthermore, our model suggested the dominance of grassland in southern Europe, which agrees with pollen reconstructions from the Mediterranean (Kageyama et al., 2005) suggesting an increase in grasslands due to a lower coldest-month temperature.

The HE1_GL simulation did not indicate major biome changes in tropical South America as compared to the LGM simulation (Fig. 11). In Northeast Brazil, the model simulated tropical forest instead of steppe and semi-desert as suggested by pollen reconstructions (Hessler et al., 2010), although the precipitation and surface air temperature decreased from LGM to HE1 (Fig. 9, top left panel and Fig. 8, top middle panel). The simulated climate of northern tropical South America (e.g. Venezuela) was drier with a maximum

Table 4. Comparison of tropical mega-biomes during the HE1 period between pollen reconstructions (compiled by Hessler et al., 2010) and model results (computed from HE1_GL using UVic ESCM). The site locations for pollen reconstruction are in tropical Africa and South America from terrestrial and marine sites (shown in Fig. 1). The blue plus sign denotes if data and model results are similar and the red plus sign denotes if data and model results are different.

No.	Latitude and Longitude	Site location name	Potential biome distribution		Comparison between data and model
			Pollen data	Model result	
equatorial Africa					
Terrestrial site					
1	3.47° S–29.57° E	Kashiru Bog, Burundi	– Grassland and dry shrubland – Savannah and xerophytic scrubland	Tropical forest	+
2	8.50° S–30.85° E	Lake Tanganyika	– Warm temperate mixed forest – Savannah and xerophytic scrubland	– Boreal forest – Savannah and dry-woodland	+
3	9.33° S–33.75° E	Lake Masoko, Tanzania	– Warm temperate mixed forest – Savannah and xerophytic scrubland	Savannah and dry-woodland	+
4	11.29° S–34.44° E	Lake Malawi	– Savannah and xerophytic scrubland – Tropical forest	Savannah and dry-woodland	+
5	4.51° N–9.40° E	Barombi Mbo, Cameroon	– Savannah and xerophytic scrubland Tropical forest	Tropical forest	+
Marine site					
6	4.40° N–4.18° W	off Ivory Coast, KS 84-063	– Tropical forest – Warm temperate mixed forest	Tropical forest	+
7	11.92° S–13.40° E	ODP 1078C – Angola	– Warm temperate mixed forest – Temperate-montane forest	– Tropical forest Temperate forest	+
8	17.15° S–11.02° E	GeoB 1023 – Cunene River Mouth	– Savannah and xerophytic scrubland – Grassland and dry shrubland	Grassland and shrubland	+
South America					
Terrestrial site					
11	2.97° S–43.42° W	Lake Caçó – NE Brazil	– Warm temperate mixed forest – Tropical forest	Tropical forest	+
12	23.87° S–46.71° W	Colônia, Brazil	– Savannah and xerophytic scrubland – Grassland and dry shrubland	– Temperate forest – Grassland and dry shrubland	+
13	17.83° S–64.72° W	Siberia, Bolivia	– Temperate-montane forest – Grassland and dry shrubland	Temperate forest	+

Table 4. Continued.

No.	Latitude and Longitude	Site location name	Potential biome distribution		Comparison between data and model
			Pollen data	Model result	
14	4.92° N–74.03° W	La Laguna, Bogotá, Colombia	– Savannah and xerophytic scrubland – Grassland and dry shrubland	Tropical forest	+
15	4.92° N–74.03° W	Fúquene, Colombia	– Savannah and xerophytic scrubland – Temperate-montane forest	Tropical forest	+
Marine site					
9	3.67° S–37.72° W	GeoB 3104 – off NE Brazil	– Temperate-montane forest – Warm temperate mixed forest	Tropical forest	+
10	4.15° S–36.21° W	GeoB 3910-2 – off NE Brazil	– Savannah and xerophytic scrubland – Warm temperate mixed forest	Tropical forest	+

precipitation anomaly of around -0.08 m yr^{-1} (Fig. 9, top left panel). However, in our simulation the tropical forest remained (Fig. 11), although biogeochemical data from this region suggest an increase in savannah cover (Jennerjahn et al., 2004), and palynological data of older Heinrich events (HE3, HE4, HE5, HE5a and HE6) also indicate an increase in savannah (Behling et al., 2000). Northwest South America received less precipitation in the HE1_GL simulation. Again, the biome distribution remained similar to the LGM simulations, while reconstructions from La Laguna de Bogotá in Colombia indicate savannah and grassland (Helmens et al., 1996). Discrepancies in northern South America indicate that climate changes of the HE1_GL simulation were not strong enough to influence the biome coverage, or that our vegetation model was not sensitive enough. On the other hand, our biome distribution in northwest Brazil of the HE1_GL simulation is in good agreement with reconstructions from Lake Caçó (Ledru et al. 2006), where tropical forests were dominant and indicate a wetter climate during the HE1 period. Furthermore, the HE1_GL simulation predicted a dominance of desert in the Middle East and western Asia and Arabia, while tundra expanded in northern Eurasia, in Siberia, and over the Tibetan Plateau.

5 Discussion

Our two equilibrium simulations represent warm and cold conditions during interglacial and glacial climates and

provide two different backgrounds for the HE1 simulations. The largest cooling in air and sea-surface temperature between the PI_CNTRL and LGM simulations in the North Atlantic Ocean was due to the presence of ice-sheets in North America. However, the most recent SST reconstruction by the MARGO project (2009) shows a more pronounced cooling in the eastern than in the western North Atlantic Ocean. The disagreement with our model results is most likely due to misplaced deepwater formation sites in the pre-industrial control experiment. Comparable mismatches have also been observed in other coupled atmospheric-ocean models simulating LGM climate (Kageyama et al., 2006).

In the tropics, the SAT difference between the PI_CNTRL and LGM simulation is $\sim 1^\circ\text{C}$ over land and $\sim 2^\circ\text{C}$ over the Atlantic Ocean, while the SST difference is $2\text{--}3^\circ\text{C}$, in agreement with the MARGO reconstruction (MARGO, 2009) and other modeling studies (e.g. Crucifix et al., 2005; Otto-Bliesner et al., 2006; Kageyama et al., 2006; Roche et al., 2007). The general agreement with reconstructions from proxy data supports that the LGM simulation delivered a suitable background climate for the Heinrich Event 1 simulations.

The warm (PI_CNTRL) and cold (LGM) background climate states also differed in the AMOC, with a reduced formation of NADW and a stronger AABW inflow into the Atlantic Ocean under LGM conditions. This is in agreement with some other model simulations (e.g. Weaver et al., 2001; Weber and Drijfhout, 2007; Kageyama et al., 2010), but at odds with others (e.g. Roche et al., 2007; cf. Otto-Bliesner

et al., 2007). Proxy data (Pa/Th ratios) from ocean sediment cores suggest a weaker AMOC strength during the LGM period (Yu et al., 1996; Marchal et al., 2000; McManus et al., 2004; Gherardi et al., 2005), although they are difficult to interpret (e.g. Roche et al., 2007). McManus et al. (2004) analyze a high accumulation core from the deep western Sub-tropical Atlantic at a depth of 4.5 km, and according to their results, the AMOC during the LGM was reduced by 30% as compared to the present day, which is in broad agreement with our LGM simulation (Figs. 2f and 5d).

The two different climatic background conditions corresponding to two different states of the AMOC did not change the predicted vegetation distribution (Figs. 4, 5a, and 6a) except in a few locations: in northern tropical Africa (the Sahel region), western South America, and central North America. For example, in central Africa, a warmer and wetter climate was predicted in the PI_CNTRL simulation as compared to the LGM simulation. This resulted in more tropical forest and savannah in the PI_CNTRL simulation, while warm-temperate forest and grassland cover were extended in the LGM simulation. In general, most changes in the vegetation encompassed rather small areas. We may suspect that the initial vegetation conditions for the vegetation model or the relative simplicity of the land-atmosphere model caused the similar vegetation cover estimates of the PI_CNTRL and LGM simulations. However, Hughes et al. (2004) showed that the TRIFFID DGVM is insensitive to the choice of the initial vegetation cover, and Meissner et al. (2003) showed that coupling the TRIFFID model to the UVic ESCM results in predicted vegetation patterns that compare reasonably well to observations.

The key climate parameters which influence vegetation cover are temperature and precipitation. Our model results from the Heinrich Event 1 simulations showed that these climate factors respond to changes in NADW formation. The AMOC reduction or collapse following the freshwater perturbation caused temperature and precipitation changes (Figs. 8 and 9), and those changes drove a subsequent response in the vegetation distribution, especially around the tropical North Atlantic, in tropical western South America, and in southwestern Asia (Fig. 10). In the HE1_GL simulation, the AMOC collapsed (Fig. 7a) and the associated heat transfer from low to high latitudes in the Atlantic Ocean was strongly reduced (in accordance with the bipolar seesaw hypothesis, Fig. 8). The inter-hemispheric thermal gradient was strengthened due to the cooling in the North Atlantic. This would be expected to shift the ITCZ in the direction of the warmer Southern Hemisphere. The precipitation in our HE1_GL simulation did not indicate a southward shift of ITCZ (Fig. 9) due to the lack of a wind feedback in our simulation. The effect of including a geostrophic wind feedback scheme is a matter of further investigation. Nevertheless, our HE1_GL simulation indicated high rainfall south of the equator, which most likely was due to the enhanced evaporation over the ocean and changes in atmospheric moisture

transport. On the other hand, the HE1_IJGL simulation indicated only a slight reduction of the AMOC strength (Fig. 7b), resulting in less pronounced climate changes (Figs. 8 and 9) and consequently less vegetation response (Fig. 10). Another problem in simulating precipitation over tropical land regions is the lack of land surface processes in the coupled land-atmospheric model (Weaver et al., 2001) and is most strongly observed in the precipitation pattern over South America. This is probably the main reason why the modeled vegetation deviates so strongly from the biome reconstructions, particularly in eastern and northeastern South America (Fig. 11).

6 Summary and conclusions

This study investigated the effects of climate change in the region of and around the tropical Atlantic during Heinrich Event 1. We presented the distribution of vegetation simulated by the UVic Earth system climate model including a dynamic vegetation module for four scenarios: pre-industrial (PI_CNTRL), freshwater perturbation of the PI_CNTRL equilibrium (HE1_IJGL), last glacial maximum (LGM), and freshwater perturbation of the LGM equilibrium simulating Heinrich Event 1 (HE1_GL). Adding freshwater to the North Atlantic resulted in a collapse of the Atlantic Meridional Overturning Circulation (AMOC), followed by a cooling of the Northern Hemisphere and a warming of the Southern Hemisphere (the bipolar seesaw hypothesis), causing a strengthening of the inter-hemispheric thermal gradient. This inter-hemispheric thermal gradient resulted in changes in rainfall patterns driving a southward shift of tropical and subtropical biomes.

The two equilibrium simulations (PI_CNTRL and LGM) allowed analyzing the response of the vegetation cover around the tropical Atlantic to a freshwater perturbation in the North Atlantic Ocean under different climatic background conditions. Our PI_CNTRL biomes were in general agreement with modern biome reconstructions. Discrepancies occurred with respect to the simulation of the dominance of grasslands in southern Europe and the failure to simulate a mixture of savannah and warm-temperate forests along the east coast of South America for the preindustrial period. The climate and biome patterns of tropical and sub-tropical South America of our LGM simulation differ from other model results (Roche et al., 2007) and a data compilation (Ray and Adams, 2001) by suggesting wetter conditions and more forest cover.

The HE1 simulations exhibited a southward shift of the southern desert boundary in northern Africa, but failed to mimic expected changes in eastern South America. The vegetation responded similarly during the HE1 simulations under interglacial (pre-industrial) and glacial (LGM) climatic background conditions, except for northern tropical Africa, western Eurasia, and western South America. The magnitude of the changes in the tree and grass PFTs is larger for

glacial than for interglacial climatic background conditions. The HE1 simulations produced a cooler climate in the Northern Hemisphere, a drier climate in northern tropical Africa and a local warming in the Southern Hemisphere, (cf. Menviel et al., 2008; Kageyama et al., 2009; Swingedouw et al., 2009). In addition, the vegetation responded to a changing climate through an increase in non-forested and desert PFT coverage in northern tropical Africa and a change from warm-temperate to tropical forests in Southwest Africa.

The biome comparison between the HE1 simulations and several data compilations for tropical Africa and South America showed reasonable agreement in vegetation patterns reconstructed from marine and terrestrial records. Limitations in the number of PFTs and modeled biomes on the one hand and the lack of precision of the palynologically reconstructed biomes on the other hand, lead to differences that are difficult to assess. Improvements in the dynamic vegetation modeling can be achieved by the addition of more PFTs and specific climatic limitations to the defined plant functional types (e.g. instead of one two broadleaved forest PFTs, a tropical and deciduous one). Nevertheless, the simulations showed that a collapse of the AMOC and the associated changes in North Atlantic climate are physically consistent with the reconstructed changes in vegetation in the tropical regions around the Atlantic Ocean during the HE1 period.

Acknowledgements. This work was funded by the Deutsche Forschungsgemeinschaft (DFG) as part of the German contribution to the Integrated Ocean Drilling Program (SPP 527) “Abrupt Climate Change in the African Tropics (ACCAT)” and the DFG Research Center/Excellence Cluster “The Ocean in the Earth System”. We thank Maria Fernanda Sanchez-Goñi and an anonymous reviewer for their helpful comments. Finally, we thank Michael Eby and the Climate Modelling Group at the University of Victoria for providing us with a copy of the UVic coupled climate model.

Edited by: M. Siddall

References

- Altabet, M. A., Higginson, M. J., and Murray, D. W.: The effect of millennial-scale changes in Arabian Sea denitrification on atmospheric CO₂, *Nature*, 415, 159–162, 2002.
- Arz, H. W., Pätzold, J., and Wefer, G.: Correlated millennial-scale changes in surface hydrography and terrigenous sediment yield inferred from last-glacial marine deposits off Northeastern Brazil, *Quaternary Res.*, 197, 323–333, 1998.
- Barker, S., Diz, P., Vautravers, M. J., Pike, J., Knorr, G., Hall, I. R., and Broecker, W. S.: Interhemispheric Atlantic seesaw response during the last deglaciation, *Nature*, 457, 1097–1101, 2009.
- Behling, H., Arz, H. W., Pätzold, J., and Wefer, G.: Late Quaternary vegetational and climate dynamics in Northeastern Brazil, inferences from marine core GeoB 3104-1, *Quaternary Sci. Rev.*, 19, 981–994, 2000.
- Berger, A. L.: Long-term variations of daily insolation and quaternary climate change, *J. Atmos. Sci.*, 35, 2362–2367, 1978.
- Bigelow, N. H., Brubaker, L. B., Edwards, M. E., Harrison, S. P., Prentice, I. C., Anderson, P. M., Andreev, A. A., Bartlein, P. J., Christensen, T. R., Cramer, W., Kaplan, J. O., Lozhkin, A. V., Matveyeva, N. V., Murray, D. V., McGuire, A. D., Razzhivin, V. Y., Ritchie, J. C., Smith, B., Walker, D. A., Gajewski, K., Wolf, V., Holmqvist, B. H., Igarashi, Y., Kremenetskii, K., Paus, A., Pisaric, M. F. J., and Vokova, V. S.: Climate change and Arctic ecosystems. I. Vegetation changes north of 55° N between the Last Glacial Maximum, mid-Holocene and present, *J. Geophys. Res.*, 108, 8170, doi:10.1029/2002JD002558, 2003.
- Bitz, C. M., Holland, M., Weaver, A. J., and Eby, M.: Simulating the ice-thickness distribution in a coupled climate model, *J. Geophys. Res.*, 106, 2441–2464, 2001.
- Bond, G., Heinrich, H., Broecker, W., Labeyrie, L., McManus, J., Andrews, J., Huon, S., Jantschik, R., Clasen, S., Simet, C., Tedesco, K., Klas, M., Bonani, G., and Ivy, S.: Evidence for massive discharges of icebergs into the North Atlantic ocean during the last glacial period, *Nature*, 360, 245–499, 1992.
- Bond, G. C., Broecker, W. S., Johnsen, S., McManus, J., Labeyrie, L., Jouzel, J., and Bonani, G.: Correlation between climate records from the North Atlantic sediment and Greenland ice, *Nature*, 365, 143–147, 1993.
- Broecker, W. S.: Massive iceberg discharges as triggers for global climate change, *Nature*, 372, 421–424, 1994.
- Broecker, W. S., Peteet, D. M., and Rind, D.: Does the ocean-atmosphere system have more than one stable mode of operation?, *Nature*, 315, 21–26, 1985.
- Broecker, W. S., Bond, G. C., Klas, M., Clark, E., and McManus, J.: Origin of the northern Atlantic’s Heinrich events, *Clim. Dynam.*, 6, 265–273, 1992.
- Chappell, J.: Sea-level changes forced ice breakouts in the Last Glacial cycle: new results from coral terraces, *Quaternary Sci. Rev.*, 21, 1229–1240, 2002.
- Chiang, J. C. H.: The Tropics in Paleoclimate, *Ann. Rev. Earth Planet. Sci.*, 37, 263–297, doi:10.1146/annurev.earth.031208.100217, 2009.
- Clark, P. U., Hostetler, S. W., Pisias, N. G., Schmittner, A., and Meissner, K. J.: Mechanisms for a ~7-kyr climate and sea-level oscillation during Marine Isotope Stage 3, in: *Ocean Circulation: Mechanisms and Impacts*, AGU, Washington, DC, Geophysical Monograph 173, 209–246, 2007.
- Collatz, G. J., Ball, J. T., Grivet, C., and Berry, J. A.: Physiological and environmental regulation of stomatal conductance, photosynthesis and transpiration: a model that includes a laminar boundary layer, *Agr. Forest Meteorol.*, 54, 107–136, 1991.
- Collins, J. A., Schefuß, E., Heslop, D., Mulitza, S., Prange, M., Zabel, M., Tjallingii, R., Dokken, T. M., Huang, E., Mackensen, A., Schulz, M., Tian, J., Zariess, M., and Wefer, G.: Interhemispheric symmetry of the tropical African rainbelt over the past 23 000 years, *Nat. Geosci.*, 4, 42–45, doi:10.1038/ngeo1039, 2011.
- Conkright, M. E., Levitus, S., O’Brien, T., Boyer, T. P., Stephens, C., Johnson, D., Stathoplos, L., Baranova, O., Antonov, J., Gelfeld, R., Burney, J., Rochester, J., and Forgy, C.: World Ocean Database 1998 Documentation and Quality Control, available at: <http://iridl.ldeo.columbia.edu/SOURCES/NOAA/NODC/WOA98/ANNUAL/>, last access: 19 April 2011, National Oceanographic Data Center, Silver Spring, MD, 1998.

- Cortijo, E., Labeyrie, L., Vidal, L., Vautravers, M., Chapman, M., Duplessy, J. C., Elliot, M., Arnold, M., Turon, J. L., and Auffret, G.: Changes in sea surface hydrology associated with Heinrich event 4 in the North Atlantic Ocean between 40° N and 60° N, *Earth Planet. Sc. Lett.*, 146, 29–45, 1997.
- Cox, P. M.: Description of the “TRIFFID” dynamic global vegetation model, Hadley Centre Technical Note 24, Met Office, Bracknell, 2001.
- Cox, P. M., Betts, R. A., Bunton, C. B., Essery, R. L. H., Rowntree, P. R., and Smith, J.: The impact of new land surface physics on the GCM simulation of climate and climate sensitivity, *Clim. Dynam.*, 15, 183–203, 1999.
- Crucifix, M., Betts, R. A., and Hewitt, C. D.: Pre-industrial-potential and Last Glacial Maximum global vegetation simulated with a coupled climate-biosphere model: diagnosis of bioclimatic relationships, *Global Planet. Change*, 45, 295–312, 2005.
- Dupont, L. M., Jahns, S., Marret, F., and Ning, S.: Vegetation change in equatorial West Africa: time-slices for the last 150 ka, *Palaeogeogr. Palaeoclimatol.*, 155, 95–122, 2000.
- Dupont, L. M., Schlütz, F., Tebow Ewah, C., Jennerjahn, T. C., Paul, A., and Behling, H.: Two-step vegetation response to enhanced precipitation in Northeast Brazil during Heinrich event 1, *Global Change Biol.*, 16, 1647–1660, 2010.
- Fanning, A. G. and Weaver, A. J.: An atmospheric energy-moisture model: climatology, interpentadal climate change and coupling to an ocean general circulation model, *J. Geophys. Res.*, 101, 15111–15128, 1996.
- Flückiger, J., Knutti, R., and White, J. W. C.: Oceanic processes as potential trigger and amplifying mechanisms for Heinrich events, *Paleoceanography*, 21, 1–11, 2006.
- Gherardi, J.-M., Labeyrie, L., McManus, J., Francois, R., Skinner, L. C., and Cortijo, E.: Evidence from the Northeastern Atlantic basin for variability in the rate of the meridional overturning circulation through the last deglaciation, *Earth Planet. Sc. Lett.*, 240, 710–723, 2005.
- González, C., Dupont, L. M., Behling, H., and Wefer, G.: Neotropical vegetation response to rapid climate changes during the last glacial period: Palynological evidence from the Cariaco Basin, *Quaternary Res.*, 69, 217–230, 2008.
- Grousset, F. E., Pujol, C., Labeyrie, L., Auffret, G., and Boelaert, A.: Were the North Atlantic Heinrich events triggered by the behaviour of the European ice sheets?, *Geology*, 28, 123–126, 2000.
- Harrison, S. P. and Prentice, I. C.: Climate and CO₂ controls on global vegetation distribution at the last glacial maximum: analysis based on palaeovegetation data, biome modelling and palaeoclimate simulations, *Global Change Biol.*, 9, 983–1004, 2003.
- Harrison, S. P., Yu, G., Takahara, H., and Prentice, I. C.: Palaeovegetation – diversity of temperate plants in East Asia, *Nature*, 413, 129–130, 2001.
- Helmens, K. F., Kuhry, P., Rutter, N. W., van der Borg, K., De Jong, A. F. M.: Warming at 18,000 yr B.P. in the tropical Andes, *Quaternary Res.*, 45, 289–299, 1996.
- Hemming, S. R.: Heinrich events: massive late pleistocene detritus layers of the North Atlantic and their global climate imprint, *Rev. Geophys.*, 42, RG1005, doi:10.1029/2003RG000128, 2004.
- Henrot, A.-J., François, L., Brewer, S., and Munhoven, G.: Impacts of land surface properties and atmospheric CO₂ on the Last Glacial Maximum climate: a factor separation analysis, *Clim. Past*, 5, 183–202, doi:10.5194/cp-5-183-2009, 2009.
- Hessler, I., Dupont, L. M., Bonnefille, R., Behling, H., González, C., Helmens, K. F., Hooghiemstra, H., Lebamba, J., Ledru, M.-P., Lézine, A.-M., Maley, J., Marret, F., and Vincens, A.: Millennial-scale changes in vegetation records from tropical Africa and South America during the last glacial, *Quaternary Sci. Rev.*, 29, 2882–2899, doi:10.1016/j.quascirev.2009.11.029, 2010.
- Hibler, W. D.: A dynamic thermodynamic sea ice model, *J. Phys. Oceanogr.*, 9, 815–846, 1979.
- Hughen, K. A., Eglinton, T. I., Xu, L., and Makou, M.: Abrupt tropical vegetation response to rapid climate changes, *Science*, 304, 955–959, 2004.
- Hughes, J. K., Valdes, P. J., and Betts, R. A.: Dynamical properties of the TRIFFID dynamic global vegetation model, Hadley Centre Technical Note 56, Met Office, Bracknell, 2004.
- Hunke, E. C. and Dukowicz, J. K.: An elastic-viscous-plastic model for sea ice dynamics, *J. Phys. Oceanogr.*, 27, 1849–1867, 1997.
- Jennerjahn, T. C., Ittekkot, V., Arz, H. W., and Behling, H.: Asynchronous terrestrial and marine signals of climate change during Heinrich Events, *Science*, 306, 2236–2239, 2004.
- Kageyama, M., Combourieu Nebout, N., Sepulchre, P., Peyron, O., Krinner, G., Ramstein, G., and Cazet, J.-P.: The Last Glacial Maximum and Heinrich Event 1 in terms of climate and vegetation around the Alboran Sea: a preliminary model-data comparison, *Comp. Rend. Geosci.*, 337, 983–992, 2005.
- Kageyama, M., Laine, A., Abe-Ouchi, A., Braconnot, P., Cortijo, E., Crucifix, M., de Vernal, A., Guiot, J., Hewitt, C. D., Kitoh, A., Marti, O., Ohgaito, R., Otto-Bliesner, B., Peltier, W. R., Rosell-Melé, A., Vettoretti, G., Weber, S. L., and MARGO Project Members.: Last Glacial Maximum temperature over the North Atlantic, Europe and western Siberia: a comparison between PMIP models, MARGO sea-surface temperatures and pollen-based reconstructions, *Quaternary Sci. Rev.*, 25, 2082–2102, 2006.
- Kageyama, M., Mignot, J., Swingedouw, D., Marzin, C., Alkama, R., and Marti, O.: Glacial climate sensitivity to different states of the Atlantic Meridional Overturning Circulation: results from the IPSL model, *Clim. Past*, 5, 551–570, doi:10.5194/cp-5-551-2009, 2009.
- Kageyama, M., Paul, A., Roche, D. M., and Van Meerbeeck, C. J.: Modelling glacial climatic millennial-scale variability related to changes in the Atlantic meridional overturning circulation: a review, *Quaternary Sci. Rev.*, 29, 2931–2956, 2010.
- Kalnay, E., Kanamitsu, M., Kistler, R., Collins, W., Deaven, D., Gandin, L., Iredella, M., Saha, S., White, G., Woollen, J., Zhu, Y., Leetmaa, A., and Reynolds, R.: The NCEP/NCAR 40-Year Reanalysis Project, *B. Am. Meteorol. Soc.*, 77, 437–471, 1996.
- Kaplan, J. O., Bigelow, N. H., Bartlein, P. J., Christensen, T. R., Cramer, W., Harrison, S. P., Matveyeva, N. V., McGuire, A. D., Murray, D. F., Prentice, I. C., Razzhivin, V. Y., Smith, B., Walker, D. A., Anderson, P. M., Andreev, A. A., Brubaker, L. B., Edwards, M. E., Lozhkin, A. V., and Ritchie, J.: Climate change and Arctic ecosystems II: Modeling, palaeodata-model comparisons, and future projections, *J. Geophys. Res.*, 108, 8171, doi:10.1029/2002JD002559, 2003.

- Köhler, P., Joos, F., Gerber, S., and Knutti, R.: Simulated changes in vegetation distribution, land carbon storage, and atmospheric CO₂ in response to a collapse of the North Atlantic thermohaline circulation, *Clim. Dynam.*, 25, 689–708, 2005.
- Lamy, F., Kaiser, J., Arz, H. W., Hebbeln, D., Ninnemann, U. S., Timm, O., Timmermann, A., and Toggweiler, J. R.: Modulation of the bipolar seesaw in the Southeast Pacific during Termination 1, *Earth Planet. Sc. Lett.*, 259, 400–413, 2007.
- Ledru, M.-P., Ceccantini, G., Gouveia, S. E. M., Lopez-Saez, J. A., Pessenda, L. C. R., and Ribeiro, A. S.: Millennial-scale climatic and vegetation changes in a northern Cerrado (Northeast, Brazil) since the Last Glacial Maximum, *Quaternary Sci. Rev.*, 25, 1110–1126, 2006.
- Loveland, T. R., Reed, B. C., Brown, J. F., Ohlen, D. O., Zhu, S., Yang, L., and Merchant, J. W.: Developments of a global land cover characteristics database and IGBP DISCover from 1 km AVHRR data, *Int. J. Remote Sens.*, 21, 1303–1330, 2000.
- Lumpkin, R. and Speer, K.: Global ocean meridional overturning, *J. Phys. Oceanogr.*, 37, 2250–2262, 2007.
- Marchal, O., François, R., Stocker, T. F., and Joos, F.: Ocean thermohaline circulation and sedimentary 231Pa/230Th ratio, *Paleoceanography*, 15, 625–641, 2000.
- MARGO Project Members: Constraints on the magnitude and patterns of ocean cooling at the Last Glacial Maximum, *Nat. Geosci.*, 2, 127–132, 2009.
- McManus, J. F., François, R., Gherardi, J.-M., Keigwin, L. D., and Brown-Leger, S.: Collapse and rapid resumption of Atlantic meridional circulation linked to deglacial climate changes, *Nature*, 428, 834–837, 2004.
- Meissner, K. J., Weaver, A. J., Matthews, H. D., and Cox, P. M.: The role of land surface dynamics in glacial inception: a study with the UVic Earth System model, *Clim. Dynam.*, 21, 515–537, 2003.
- Menviel, L., Timmermann, A., Mouchet, A., and Timm, O.: Meridional reorganizations of marine and terrestrial productivity during Heinrich events, *Paleoceanography*, 1–19, PA1203, doi:10.1029/2007PA001445, 2008.
- Mulitza, S., Prange, M., Stuut, J.-B., Zabel, M., Dobeneck, T. V., Itambi, A. C., Nizou, J., Schulz, M., and Wefer, G.: Sahel megadroughts triggered by glacial slowdowns of Atlantic meridional overturning, *Paleoceanography*, 23, 1–11, PA4206, doi:10.1029/2008PA001637, 2008.
- Otto-Bliesner, B. L., Brady, E. C., Clauzet, G., Tomas, R., Levis, S., and Kothavala, Z.: Last Glacial Maximum and Holocene Climate in CCSM3, *J. Climate*, 19, 2526–2544, 2006.
- Otto-Bliesner, B. L., Hewitt, C. D., Marchitto, T. M., Brady, E., Abe-Ouchi, A., Crucifix, M., Murakami, S., and Weber, S. L.: Last Glacial Maximum ocean thermohaline circulation: PMIP2 model intercomparisons and data constraints, *Geophys. Res. Lett.*, 34, 1–6, L12706, doi:10.1029/2007GL029475, 2007.
- Pacanowski, R. C.: MOM 2 Documentation: Users Guide and Reference Manual, Version 1.0, GFDL Ocean Group Technical Report No. 3, Geophysical Fluid Dynamics Laboratory, Princeton, New Jersey, 1995.
- Peltier, W. R.: Global Glacial Isostasy and the Surface of the Ice-Age Earth: The ICE-5G (VM2) Model and GRACE, Invited paper, *Annu. Rev. Earth Planet. Sci.*, 32, 111–149, doi:10.1146/annurev.earth.32.082503.144359, 2004.
- Peterson, L. C., Haug, G. H., Hughen, K. A., and Röhl, U.: Rapid changes in the hydrologic cycle of the tropical Atlantic during the last glacial, *Science*, 290, 1947–1951, 2000.
- Pickett, E., Harrison, S. P., Hope, G., Harle, K., Dodson, J. R., Kershaw, A. P., Prentice, I. C., Backhouse, J., Colhoun, E. A., D’Costa, D., Flenley, J., Grindrod, J., Haberle, S., Hassell, C., Kenyon, C., Macphail, M., Martin, H., Martin, A. H., McKenzie, M., Newsome, J. C., Penny, D., Powell, J., Raine, I., Southern, W., Stevenson, J., Sutra, J.-P., Thomas, I., van der Kaars, S., and Ward, J.: Pollen-based reconstructions of biome distributions for Australia, South East Asia and the Pacific (SEAPAC region) at 0, 6000 and 18 000 14C yr BP, *J. Biogeogr.*, 31, 1381–1444, 2004.
- Prentice, I. C. and Webb III, T.: BIOME 6000: reconstructing global mid-Holocene vegetation patterns from paleoecological records, *J. Biogeogr.*, 25, 997–1005, 1998.
- Prentice, I. C., Cramer, W., Harrison, S. P., Leemans, R., Monserud, R. A., and Solomon, A. M.: A global biome model based on plant physiology and dominance, soil properties and climate, *J. Biogeogr.*, 19, 117–134, 1992.
- Prentice, I. C., Jolly, D., and BIOME 6000 Members.: Mid-Holocene and glacial-maximum vegetation geography of the northern continents and Africa, *J. Biogeogr.*, 27, 507–519, 2000.
- Ray, N. and Adams, J. M.: A GIS-based Vegetation Map of the World at the Last Glacial Maximum (25 000–15 000 BP), *Internet Archaeology*, available at: <http://intarch.ac.uk/journal/issue11/rayadams.toc.html> (last access: 19 April 2011), 2001.
- Roche, D. M., Dokken, T. M., Goosse, H., Renssen, H., and Weber, S. L.: Climate of the Last Glacial Maximum: sensitivity studies and model-data comparison with the LOVECLIM coupled model, *Clim. Past*, 3, 205–224, doi:10.5194/cp-3-205-2007, 2007.
- Schmitter, A., Meissner, K. J., Eby, M., and Weaver, A. J.: Forcing of the deep ocean circulation in simulations of the Last Glacial Maximum, *Paleoceanography*, 17, 1015, doi:10.1029/2001PA000633, 2002.
- Scholze, M., Knorr, W., and Heimann, M.: Modelling terrestrial vegetation dynamics and carbon cycling for an abrupt climatic change event, *Holocene*, 13, 327–333, 2003.
- Swingedouw, D., Mignot, L. J., Braconnot, P., Mosquet, E., Kageyama, M., and Alkama, R.: Impact of freshwater release in the North Atlantic under different climate conditions in an OAGCM, *J. Climate*, 22, 6377–6401, 2009.
- Vidal, L., Labeyrie, L., Cortijo, E., Arnold, M., Duplessy, J., Michel, E., Becque, S., and van-Weering, T.: Evidence for changes in the North Atlantic DeepWater linked to meltwater surges during the Heinrich events, *Earth Planet. Sc. Lett.*, 146, 13–27, 1997.
- Weaver, A. J., Eby, M., Wiebe, E. C., Bitz, C. M., Duffy, P. B., Ewen, T. L., Fanning, A. F., Holland, M. M., MacFadyen, A., Matthews, H. D., Meissner, K. J., Saenko, O., Schmittner, A., Wang, H., and Yoshimori, M.: The UVic Earth System Climate Model: model description, climatology, and applications to past, present and future climates, *Atmos.–Ocean*, 39, 361–428, 2001.
- Weaver, A. J., Saenko, O. A., Clark, P. U., and Mitrovica, J. X.: Meltwater pulse 1A from Antarctica as a trigger of the Bølling-Allerød warm interval, *Science*, 299, 1709–1713, 2003.

- Weber, S. L. and Drijfhout, S. S.: Stability of the Atlantic meridional overturning circulation in the Last Glacial maximum climate, *Geophys. Res. Lett.*, 34, L22706, doi:10.1029/2007GL031437, 2007.
- Yokoyama, Y., De Deckker, P., Lambeck, K., Johnston, P., and Field, L. K.: Sea-level at the last glacial maximum: evidence from northwestern Australia to constrain ice volumes for oxygen isotope stage 2, *Palaeogeogr. Palaeoclimatol.*, 165, 281–297, 2001.
- Yu, E. F., Francois, R., and Bacon, M. P.: Similar rates of modern and last-glacial ocean thermohaline circulation inferred from radiochemical data, *Nature*, 379, 689–694, 1996.